frontiers | Frontiers in Chemistry

TYPE Original Research
PUBLISHED 26 July 2024
DOI 10.3389/fchem.2024.1425693

OPEN ACCESS

EDITED BY
Shuang Fang Lim,
North Carolina State University, United States

REVIEWED BY
Niravkumar J. Joshi,
University of Barcelona, Spain
Yutong Han,
University of Shanghai for Science and Technology, China

*CORRESPONDENCE
Juanjuan Hao,
jyhao@hit.edu.cn
You Wang,
y-wang@hit.edu.cn

†These authors have contributed equally to this work and share first authorship

RECEIVED 30 April 2024
ACCEPTED 11 June 2024
PUBLISHED 26 July 2024

CITATION
Yi S, Chen C, Yu M, Hao J and Wang Y (2024), 2D/2D $Bi_2Se_3/SnSe_2$ heterostructure with rapid NO_2 gas detection.
Front. Chem. 12:1425693.
doi: 10.3389/fchem.2024.1425693

2D/2D $Bi_2Se_3/SnSe_2$ heterostructure with rapid NO_2 gas detection

Shuangshuang Yi†, Cunguang Chen†, Meiling Yu, Juanjuan Hao* and You Wang*

School of Materials Science and Engineering, Harbin Institute of Technology, Harbin, China

Heterostructure engineering is crucial for enhancing gas sensing performance. However, achieving rapid response for room-temperature NO_2 sensing through rational heterostructure design remains a challenge. In this study, a $Bi_2Se_3/SnSe_2$ 2D/2D heterostructure was synthesized by hydrothermal method for the rapid detection of NO_2 at room temperature. By combining Bi_2Se_3 nanosheets with $SnSe_2$ nanosheets, the $Bi_2Se_3/SnSe_2$ sensor demonstrated and the lowest detection limit for NO_2 a short response time (15 s) to 10 ppm NO_2 at room temperature, reaches 25 ppb. Furthermore the sensor demonstrates significantly larger response to NO_2 than to other interfering gases, including 10 ppm NO_2, H_2S, NH_3, CH_4, CO, and SO_2,demonstrating its outstanding selectivity. And we discuss the mechanism of related performance enhancement.

KEYWORDS

2D, NO_2 Sensing, heterostructure, room-temperature, flexible sensor

1 Introduction

Flexible sensors for pressure, temperature, humidity, strain, and heat flux have garnered significant attention in the fields of electronic skin, environmental monitoring, and body temperature monitoring (Ansari et al., 2023). Gas sensing has become a critical aspect in atmospheric environment monitoring, industrial production, and medical healthcare applications (Yang et al., 2023).NO_2 stands as one of the most prevalent air pollutants. Studies indicate that even brief exposure to concentrations as low as 3 ppm can cause eye and lung irritation in human, while also compromising respiratory infection resistance, potentially resulting in fatality in severe cases (Spirtas et al., 1986; Qureshi et al., 2003; Rathi and Pal 2020).Therefore, the development of highly responsive and rapid gas sensing technologies for the detection of low-concentration NO_2 at routine temperatures assumes paramount importance in practical applications.

Two-dimensional metal chalcogenides (TMDs) have attracted considerable interest in gas sensing owing to their superior electrical properties, large surface area, and abundant adsorption sites (Zheng et al., 2016; Sardana et al., 2022; Yang et al., 2022; Wang et al., 2023; Yang et al., 2024).Huang et al. modified two-dimensional material MoS_2 with zinc oxide nanoparticles to improve the response of MoS_2 to NO_2 (Han et al., 2018).While tin (Sn) is not classified as a transition metal, its selenide compound can adopt a 2D-layered hexagonal structure similar to that of TMDs (D'Olimpio et al., 2022; Harish and Sathyakam, 2022). Moreover heterostructures offer significant potential for a broad applications, including high-speed electronics and optoelectronic devices. By integrating SnS_2 nanosheets with the $Ti_3C_2T_x$ skeleton platform, Han et al. achieved a good response to 50ppm triethylamine at room temperature (Han et al., 2023). So the fabrication of heterostructures has been widely utilized

to further enhance the sensing performance of gas sensors based on $SnSe_2$. For instance, Li et al. fabricated a chemiresistive sensor based on a $SnSe_2/SnO_2$ heterojunction using the thermal oxidation method for the detection of NO_2 gas (Li et al., 2020). While significant advancements have been achieved in enhancing the sensing capabilities of $SnSe_2$ for NO_2 detection, there is still a need for further improvement, particularly in terms of reducing the response time, as well as improving selectivity. An important limitation of two-dimensional materials for room temperature gas sensing is the long response recovery time due to the slow desorption process. It is well understood that in comparison to 0D/2D and 1D/2D heterostructures, 2D/2D heterostructures offer closer interfacial contacts, facilitating enhanced charge transfer and thereby improving sensing properties. It is anticipated that the development of these 2D/2D heterostructures on $SnSe_2$ could efficiently accelerate the response time.

Enhancing selectivity is a critical factor for gas sensing equipment. Current strategies employed to improve the selectivity of gas sensing devices encompass precious metal modification, heterostructural construction, ultraviolet irradiation, and external auxiliary heatin (Majhi et al., 2015; Zhang et al., 2016; Joshi et al., 2018) Bi_2Se_3, a representative 2D semiconductor, has gained significant interest across various fields like optoelectronic circuit, photocatalysis, and batteries due to its favorable bandgap, exceptional stability, and ease of synthesis (Huang et al., 2020; Li et al., 2022). Moreover, the lower work function of Bi_2Se_3 compared to $SnSe_2$ promotes facilitates electron migration from Bi_2Se_3 to $SnSe_2$, resulting in a decrease in the work function of $SnSe_2$. This reduced work function of $SnSe_2$ facilitates electron transfer to NO_2 molecules during sensing (Li et al., 2024). Additionally, the remarkable catalytic properties of Bi_2Se_3 contribute to lowering the activation energy needed for gas sensing, ultimately enhancing sensing performance, particularly in reducing response time and increasing selectivity. Consequently, the engineering of 2D/2D heterostructures by combining Bi_2Se_3 nanosheets and $SnSe_2$ holds promise for developing sensors with improved sensitivity and rapid response at room temperatures.

In this study, 2D/2D heterostructures of $SnSe_2/Bi_2Se_3$ were synthesized using a combination of colloidal method and solvothermal method with a laminated stack structure. The optimized $SnSe_2/Bi_2Se_3$ sensor demonstrated a notable reduction in response time for 10 ppm NO_2, dropping from 73 to 15 s, and a

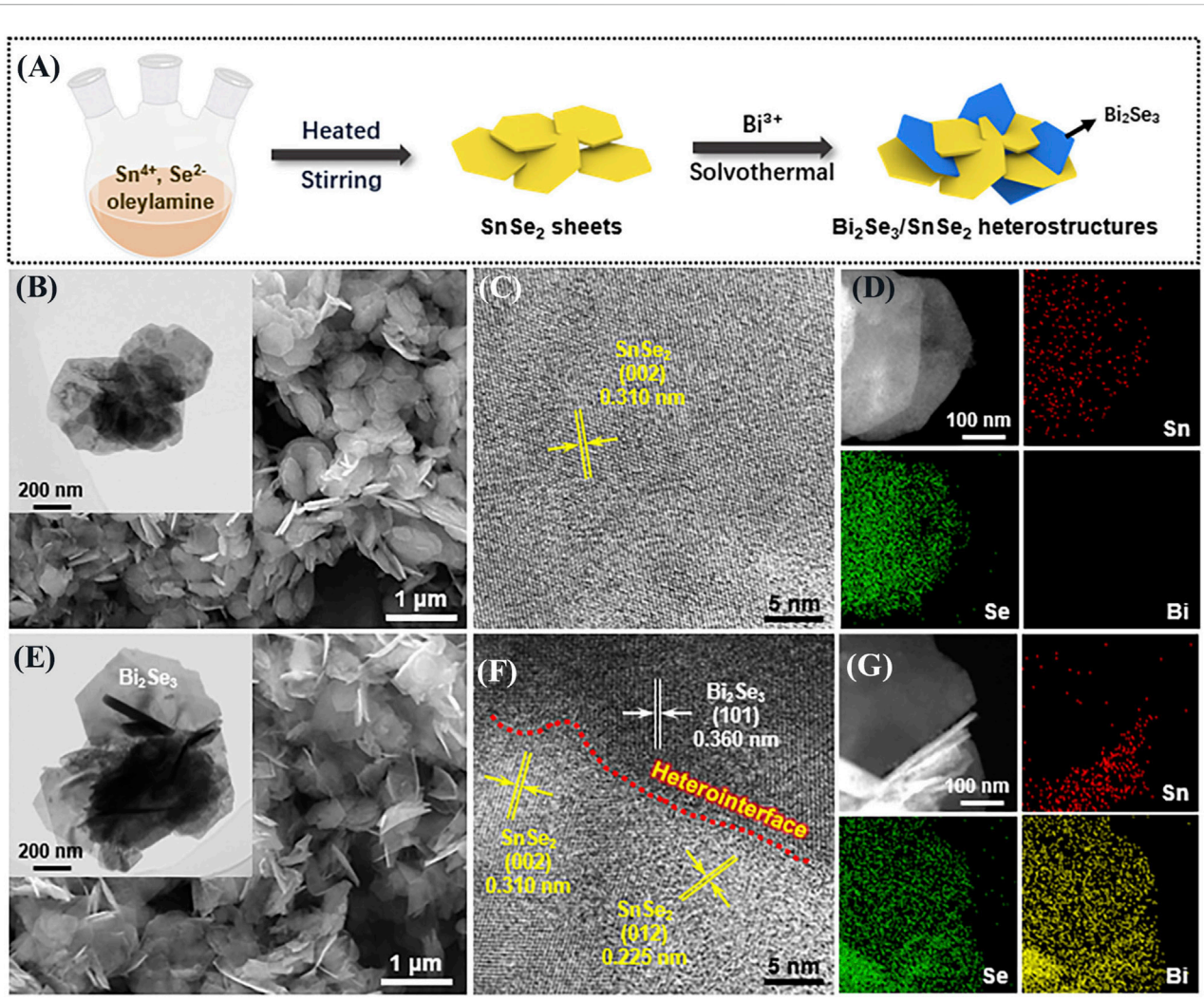

FIGURE 1
(A) Diagram showing the synthetic process of $Bi_2Se_3/SnSe_2$ heterostructure; SEM, TEM, HRTEM images, and EDX elemental mapping of **(B–D)** $SnSe_2$ and **(E–G)** $Bi_2Se_3/SnSe_2$ heterostructure.

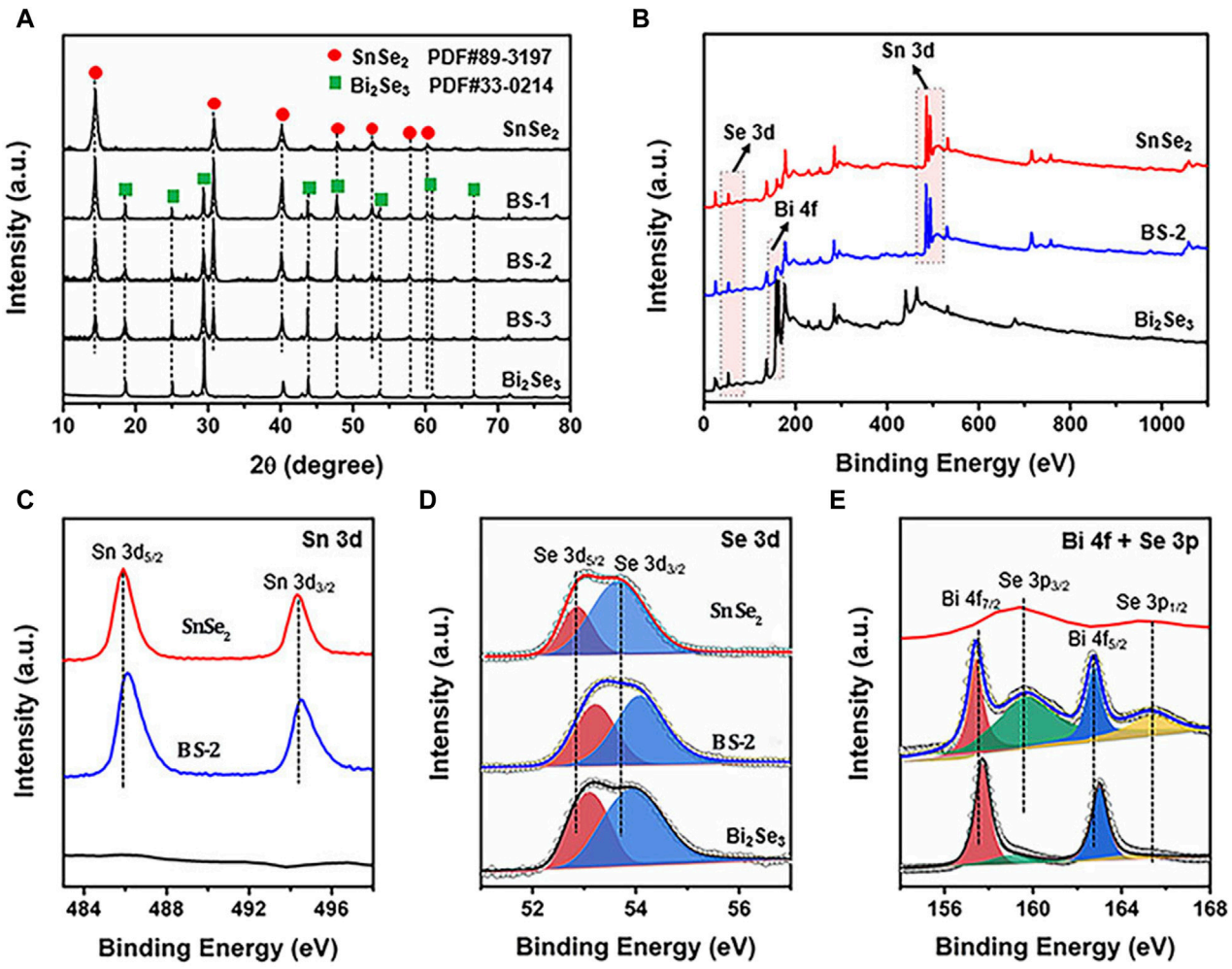

FIGURE 2
(A) XRD patterns of $SnSe_2$, Bi_2Se_3, and $SnSe_2/Bi_2Se_3$ heterostructure; XPS spectra of $SnSe_2$, Bi_2Se_3 and BS-2 samples: **(B)** Survey, **(C)** Sn 3d, **(D)** Se 3d, and **(E)** Bi 4f and Se 3p.

decrease in recovery time from 300 to 110 s. The optimized sensor also exhibits a high response to NO_2, with a high response rate of 130% to 10ppm of NO_2. These improved sensing capabilities can be ascribed to enhanced transfer of charges and the larger number of adsorption sites, which are both enabled by the $SnSe_2/Bi_2Se_3$ 2D/2D heterostructures. Additionally, the fatigue tests of the sensor after 100, 500, and 1,000 cycles of bending and relaxation showed no significant decrease in response values, demonstrating its excellent mechanical performance. These findings present a novel and effective strategy for developing a practical NO_2 gas sensor based on $SnSe_2$.

2 Materials and methods

2.1 Synthesis of $SnSe_2$ nanoplates

Firstly, 0.5 mmol $SnCl_4{\cdot}5H_2O$, 1.5 mmol SeO_2, and 0.5 mmol 1, 10 -phenanthroline were dissolved in a three-neck flask. The mixture was stirred for 10 min under a highly pure N_2 atmosphere at room temperature. Following a 10-min N_2 degassing, the solution underwent heating to 110 °C while being stirred magnetically for an additional 10 min. Then, further increased to 260 °C and maintained for another 30 min with continuous stirring. Cooling down to room temperature, the resulting products were collected and centrifuged under three rounds of washing: first with cyclohexane and then with ethanol. Ultimately, the products were kept at 70°C for 10 h.

2.2 Synthesis of $Bi_2Se_3/SnSe_2$ heterostructures

The preparation of $Bi_2Se_3/SnSe_2$ heterostructures involved a simple solvothermal method. Its synthesis process is shown in Figure 1A. Precisely, 0.2 mmol of the pre-synthesized $SnSe_2$ was gently dispersed in 20 mL ethanol and stirred for 0.5 h. Subsequently, a specific quantity of $Bi(NO_3)_3{\cdot}5H_2O$ was added to the suspension and vigorously stirred for another 0.5 h. The resulting mixture was then moved to a 25 mL Teflon-lined

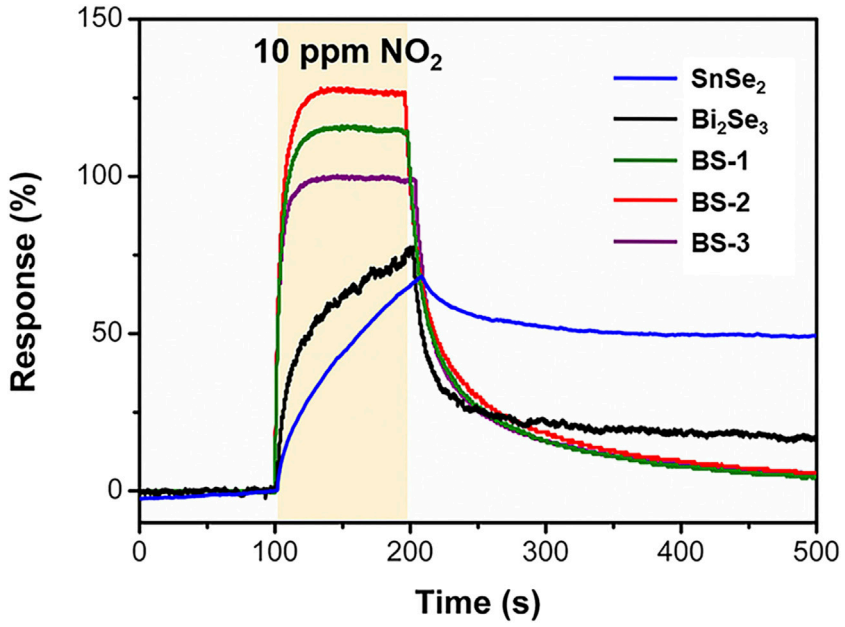

FIGURE 3
Response curves of the sensors based on $SnSe_2$, Bi_2Se_3 and $Bi_2Se_3/SnSe_2$ heterostructures to 10 ppm NO_2 at room-temperature.

autoclave and the solvothermal reaction was performed at 180 °C for 12 h. Finally, the resulting product was collected and subjected to three washes with ethanol and water.

For simplicity, the $Bi_2Se_3/SnSe_2$ heterostructures were labeled as BS-1, BS-2, and BS-5, reflecting the amounts of Bi salt added (0.020, 0.025, and 0.040 mmol) respectively. In contrast, the synthesis of pure Bi_2Se_3 involved the addition of 1 mmol Bi_2O_3, 3 mmol SeO_2, and 0.4 g NaOH into 40 mL of ethylene glycol. After being vigorously stirred for 1 h, the resulting suspension was placed in a Teflon-lined autoclave and the reaction was performed at 180°C for 7 h. Subsequently, the resultant products were collected, subjected to multiple washes with ethanol and deionized water, and finally dried at 60°C for 10 h.

2.3 Characterization of materials

The morphologies of the samples were inspected using both FESEM (SIRION 200) and TEM (JEOL-1400). Elemental composition was characterized by EDX and elemental mapping, while crystal structure was analyzed by XRD measurements (Bruker D8 Advance). The chemical states were determined through XPS analysis using an ESCALAB 250 spectrometer.

2.4 Gas-sensing properties

The gas sensors were produced through applying a solution of sensing materials through drop-casting (10 mg/mL in ethanol) onto Ag-Pd interdigital electrodes on an alumina substrate measuring 6.6 × 6.0 mm. To evaluate the gas sensing performance, a homemade sensor-testing system was employed, and a simplified experimental setup is depicted in Supplementary Figure S1. The real-time changes in conductivity of the sensors was collected via the electrochemical workstation (CHI 630E). In the sensing experiments, a precise volume of test gas was injected into the 4 L test chamber via a syringe. The relative humidity levels were regulated using a CK-80G commercial humidity chamber by Kingjo. All tests were performed in room air at 25°C with a relative humidity of 40%–50%. The sensing response (S) was determined using the equation of $S = (R_g\text{-}R_a)/R_a$, where R_g and R_a represented the sensor resistance in the target gas and in air, respectively. The response and recovery times represent the duration it takes for the sensor to reach 90% of the resistance change after a target gas was injected and released, respectively.

2.5 Manufacturing of flexible chemical sensor

The flexible chemical sensor, incorporating $Bi_2Se_3/SnSe_2$ heterostructures, was intricately applied to a polyethylene terephthalate substrate with interdigital gold patterns. The fabrication procedure for the device is meticulous and mirrors a method similar to the one previously documented. (Wang et al., 2016; Wang et al., 2017).

3 Results and discussion

3.1 Material structure and morphology

Characterized by SEM, TEM, and HRTEM. Figures 1B, E display the SEM images of $SnSe_2$ and BS-2 samples, respectively, and their insets are the corresponding TEM images. The $SnSe_2$ exhibits nanoplates morphology with the uniform dimension of

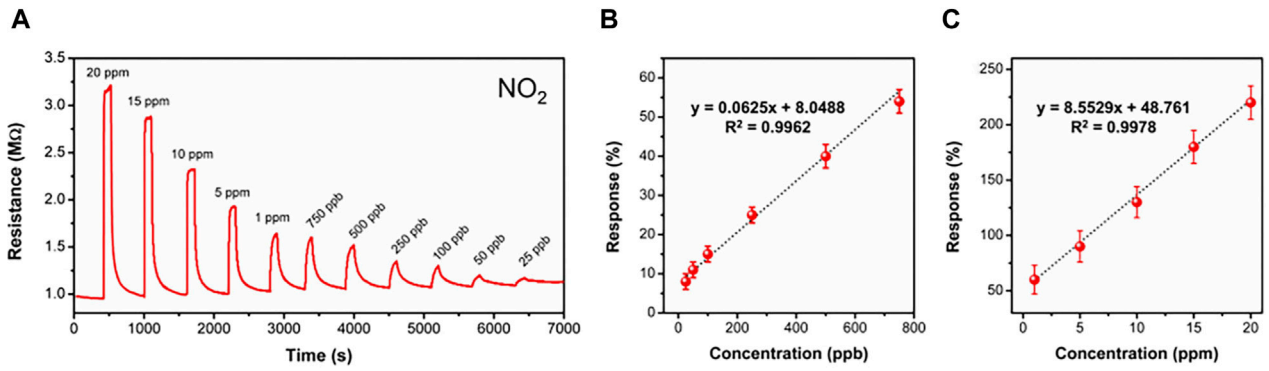

FIGURE 4
(A) Dynamic response curves of BS-2 sensor to NO_2 (20 ppm–25 ppb); **(B, C)** The correlation between gas concentration and sensor response value.

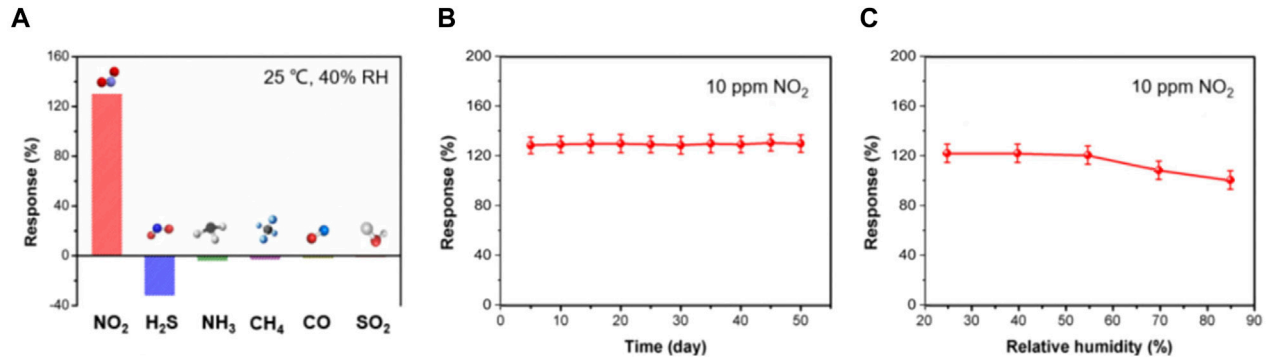

FIGURE 5
(A) Selective responses of BS-2 sensor to 10 ppm NO_2, H_2S, NH_3, CH_4, CO and SO_2; **(B)** Long-term stability and **(C)** effects of humidity on the sensing responses of BS-2 sensor to 10 ppm NO_2.

TABLE 1 Comparison of NO_2 responses of $Bi_2Se_3/SnSe_2$ sensor with that of other materials reported in literature.

Sensing materials	Working temperature/°C	Response (%)/concentration (ppm)	Detection limit/ppb	T_{res}/ T_{rec} (s)	References
MoS_2 nanosheets	25	24.8/10	1,000	50/234	Liu et al. (2020)
trilayer WSe_2	25	<64/10	/	-/-	Guo et al. (2019)
WSe_2/WS_2	25	66/10	—	-/1,500	Kim et al. (2020)
WSe_2/MoS_2	25	25/500	—	-/-	Kim et al. (2020)
This work	25	230/10	25	15/110	

500–800 nm. After the solvothermal process, the $SnSe_2$ still retain its original shape, and the hexagonal Bi_2Se_3 nanoplates grow on the surface of $SnSe_2$, forming a heterostructure with intimate contact. The HRTEM images in Figures 1C, F clearly demonstrate the presence of a heterojunction interface. The lattice spacings of 0.310 and 0.225 nm belong to the (002) and (012) planes of $SnSe_2$, respectively, while the 0.360 nm spacing corresponds to the (101) plane of Bi_2Se_3. In addition, the EDX mapping results demonstrate the uniform distribution of Sn, Se, and Bi elements (Figures 1D, G), which further indicates the formation of interconnected structures between $SnSe_2$ and Bi_2Se_3.

A control sample of nanoplate-like Bi_2Se_3 was synthesized employing a solvothermal method for comparative analysis (Supplementary Figure S2). The crystalline characteristics of $SnSe_2$, Bi_2Se_3, and the $Bi_2Se_3/SnSe_2$ heterostructures were investigated via XRD analysis, with the resulting patterns depicted in Figure 2A. The diffraction peaks observed in the pristine samples were unambiguously assigned to hexagonal $SnSe_2$ (JCPDS 89-3197) and hexagonal Bi_2Se_3 (JCPDS 33-0214). Specifically, the well-aligned distinct peaks at 14.41°, 30.73°, 40.08°, 47.69°, 52.57°, 57.81°, and 64.00° corresponded favorably to the (001), (011), (012), (110), (103), (201), and (202) crystallographic

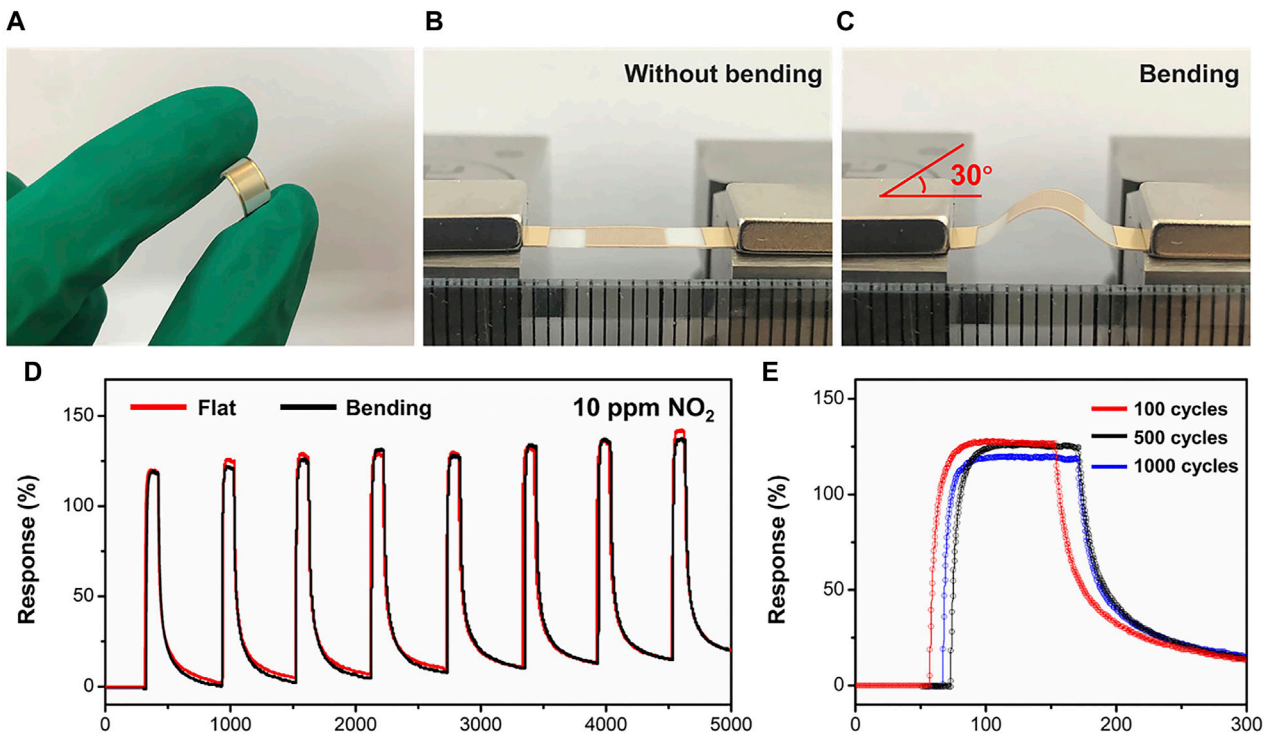

FIGURE 6
(A–C) Optical images of the flexible gas sensing device before and after bending; **(D)** Response/recovery curves of the flexible sensor without and with bending to 10 ppm NO_2; **(E)** Gas sensing stability measured after 100, 500, and 1,000 bending cycles for NO_2.

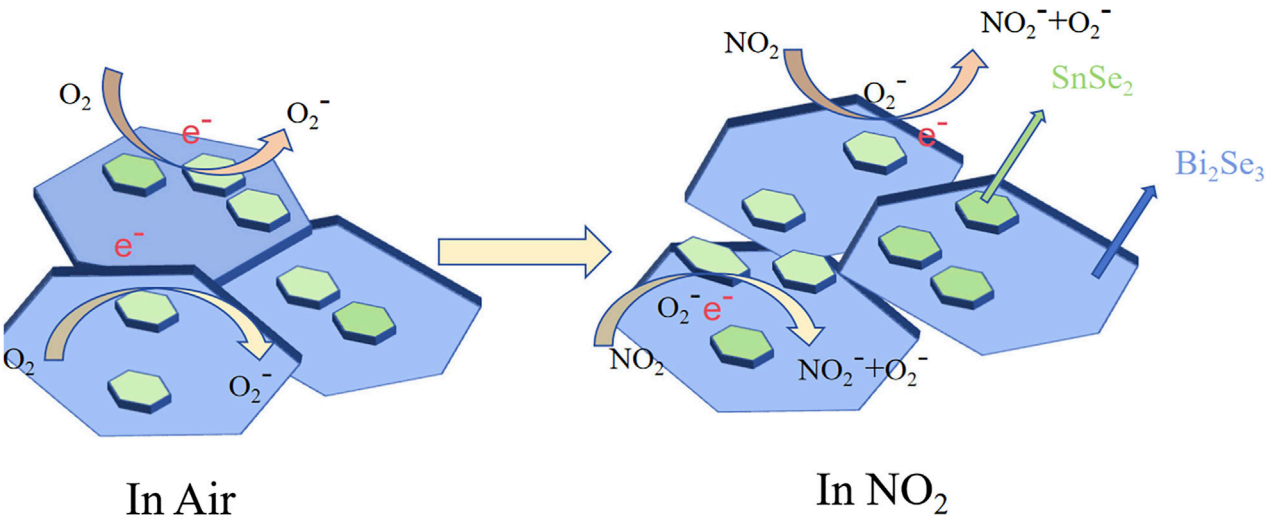

FIGURE 7
The gas sensing mechanism diagrams of $Bi_2Se_3/SnSe_2$ sensors.

planes of $SnSe_2$, respectively. Similarly, the peaks observed at 18.56°, 25.00°, 29.36°, 43.69°, 47.84°, and 53.54° were unequivocally attributed to the (006), (012), (015), (110), (116), and (205) crystallographic planes of Bi_2Se_3. With respect to the $Bi_2Se_3/SnSe_2$ heterostructures, an increase in the amount of added Bi salt led to an augmentation in the diffraction peaks of Bi_2Se_3 and a simultaneous decrease in the peak assigned to $SnSe_2$, without any noticeable impurities, thus indicating the high purity of these synthesized products.

XPS measurement was performed to analyze the chemical compositions and chemical states of the samples. The survey spectra of the BS-2 sample demonstrates the co-existence of Sn,

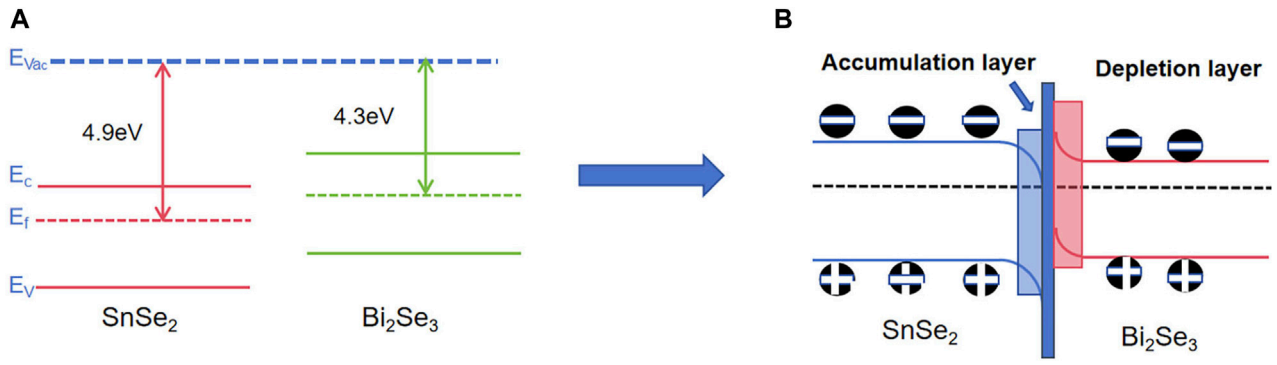

FIGURE 8
Schematic energy band diagram of $SnSe_2/Bi_2Se_3$ heterostructure **(A)** before equilibrium; **(B)** After balancing.

Se, and Bi elements (Figure 2B), which is in line with the findings from the EDX mapping. In the detailed XPS spectrum of Sn3d, peaks at 485.9 and 494.3 eV are corresponding to Sn $3d_{5/2}$ and Sn $3d_{3/2}$ (Figure 2C), respectively, indicating the presence of Sn^{4+} in $SnSe_2$. Two peaks around 52.8 and 53.6 eV belong to the $3d_{5/2}$ and $3d_{3/2}$ of Se^{2-} species (Figure 2D), respectively. In the Bi 4f and Se 3p spectra presented in Figure 2E, the distinctive peaks at 157.8 and 162.8 eV are indicative of Bi $4f_{7/2}$ and Bi $4f_{5/2}$, respectively, indicating the chemical state of Bi^{3+}. The peaks that located at 159.7 and 165.4 eV could be separately assigned to the Se $3p_{3/2}$ and Se $3p_{1/2}$ orbitals of Se^{2-} (Xu et al., 2019). Notably, in comparison with pristine $SnSe_2$, the binding energy of Sn 3d in BS-2 slightly shifts to higher energy, while the binding energy of Bi 4f in BS-2 are slightly lower than that of pure Bi_2Se_3. Such migration shifts of the binding energies may be ascribed to the change in electron density on the surfaces of the samples, and the above results confirm that the electrons in the heterostructure transfer from $SnSe_2$ to Bi_2Se_3. The analyses conducted affirm the successful creation of $Bi_2Se_3/SnSe_2$ heterostructures.

3.2 Gas sensing properties

The NO_2 sensing capabilities of $Bi_2Se_3/SnSe_2$ heterostructures were examined through testing the change in resistance upon exposed to target gases. The initial investigation focused on assessing the influence of the Bi_2Se_3 to $SnSe_2$ ratio on the sensing performance of the heterostructures. As the ratio of Bi_2Se_3 increased, the sensing response increases first then decreased (Figure 3). The BS-2 performs the most significant sensing response to NO_2. By contrast, the sensors based on pure $SnSe_2$ and Bi_2Se_3 exhibit inadequate response and sluggish recovery. The significantly improved sensing performance may be credited to the formed heterointerface between $SnSe_2$ and Bi_2Se_3, which facilitates charge transfer and provides abundant active sites. According to the detailed sensing characteristics outlined in Supplementary Table S1, the $Bi_2Se_3/SnSe_2$-2 sensor has been chosen for further research due to its impressive performance, showing the largest response rate of 130% and the shortest response/recovery times of 15/110 s to 10 ppm NO_2.

The dynamic response curve of BS-2 sensor toward different NO_2 concentration was further measured. As illustrated in Figure 4A, the sensor shows excellent response and recover ability, and the lowest detection limit for NO_2 reaches 25 ppb. Besides, the correlation equation relating response value to gas concentration at ppb (Figure 4B) and ppm level (Figure 4C) could be separately calculated as a good linear relationship, which suggests its promising potential for sensor calibration purpose. Additionally, the wide detection range of the BS-2 sensor enables it to have a broad range of applications.

The selectivity of the BS-2 sensor was studied upon exposure to different analytes, including 10 ppm NO_2, H_2S, NH_3, CH_4, CO, and SO_2. As shown in Figure 5A, the sensor demonstrates significantly larger response to NO_2 than to other interfering gases, demonstrating its outstanding selectivity. To assess long-term stability, the responses of the BS-2 sensor to 10 ppm NO_2 were recorded at a 5-day interval. The sensor exhibits a slight response recession (Figure 5B) and nearly identical sensing behaviors toward target gases within 50 days (Supplementary Figure S3), thereby affirming its significant stability and reliability. In addition, the BS-2 sensor presents notable stability when working in moderate humidity levels (25%–55%), making it suitable for practical applications (Figure 5C).

For a comprehensive assessment of sensing ability, Table 1 sums up a comparison between the optimal sensor in this study and other reported sensors based on 2D materials. The $Bi_2Se_3/SnSe_2$ sensor shows superior NO_2 sensing performance, featuring minimal power usage and heightened sensitivity, and notable response/recovery characteristics.

The sensor based on $Bi_2Se_3/SnSe_2$ demonstrates outstanding NO_2 sensing performance, showcasing minimal power usage and heightened sensitivity and remarkable response/recovery characteristics. To explore the potential capability, the mechanical flexibility properties of the BS-2 sensor were further studied. The flexible gas sensor was produced by depositing the $Bi_2Se_3/SnSe_2$ heterostructures onto a PET substrate with gold interdigitated electrodes (Figures 6A–C). The gas sensing characteristics of the sensor under bending angle of 30° were then determined. As displays in Figure 6D the dynamic response and recovery curves in each trial are consistent with the flat condition. Furthermore, the fatigue test of the sensor after 100, 500, and 1,000 cycles bending and relaxing processes shows no significant degradation in response values (Figure 6E). The results presented above showcase the promising

application potential of the flexible $Bi_2Se_3/SnSe_2$ sensor in wearable sensing devices.

3.3 Gas sensing mechanism

The gas sensing mechanism of semiconductive materials is established on the modification of resistance caused by the interaction between gas molecules and the sensing materials. (Zappa et al., 2018; Bag and Lee, 2019). The sensing mechanism of $SnSe_2$ has been extensively discussed in the literature. As depicted in Figure 7, when exposed to air, O_2 molecules adhere to the surface of n-type $SnSe_2$, resulting in the creation of O^{2-} (ads) by capturing free electrons from the conduction band of $SnSe_2$. At temperatures below 100°C, the main form of adsorbed oxygen is O^{2-}.The redox reaction described above is illustrated in Eq. 1. (Kim et al., 2017).

$$O_2(\text{gas}) + e^- \rightarrow O^{2-}(\text{ads}) \quad (1)$$

When $SnSe_2$ is exposed to NO_2, the gas molecules can efficiently capture electrons from the conduction band of $SnSe_2$ owing to the greater electronegativity of NO_2 in comparison to O_2. Furthermore, the reaction process can be delineated by Eqs 2, 3 below. Nevertheless, unmodified $SnSe_2$ demonstrates a diminished response when compared to $Bi_2Se_3/SnSe_2$. This phenomenon arises from the relatively low coverage of chemisorbed oxygen on the pristine $SnSe_2$ surface. Consequently, NO_2 can directly withdraw electrons from $SnSe_2$. (Li et al., 2020). As a result, physical adsorption (Eq. 3) predominantly influences the sensing process.

$$NO_2(\text{gas}) + e^- \rightarrow NO_2^-(ads) \quad (2)$$

$$NO_2(\text{gas}) + O_2^-(ads) + 2e^- \rightarrow NO_2^-(ads) + 2O^-(ads) \quad (3)$$

The superior NO_2 sensing properties of $Bi_2Se_3/SnSe_2$ heterostructures are primarily attributed to the following factors building upon the foundational sensing mechanism discussed earlier:

Initially, the created n–n heterojunction between Bi_2Se_3 and $SnSe_2$ plays a vital part in boosting the sensing response of the heterostructures. The electronic effects resulting from the construction of the $SnSe_2/Bi_2Se_3$ heterojunction heterostructure are primarily attributed to band alignment. As depicted in Figure 8, the work function of Bi_2Se_3 is 4.3 eV, while the work function of $SnSe_2$ is 4.9 eV. Therefore, the Fermi level of Bi_2Se_3 is notably higher than that of $SnSe_2$. Consequently, upon the formation of the heterojunction, electrons transfer from Bi_2Se_3 to $SnSe_2$, and holes transfer from $SnSe_2$ to Bi_2Se_3, leading to the separation of holes and electrons. This results in the generation of an electron accumulation layer on the $SnSe_2$ side and an electron depletion layer on the Bi_2Se_3 side, leading to electron accumulation on one side of $SnSe_2$ and an improvement in the electronic structure at the interface.

During the sensing process of NO_2 gas-sensitive materials, when NO_2 gas molecules come into contact with the material surface in a detection gas environment, the gas is first adsorbed by the material. Due to the oxidizing nature of NO_2, it then captures electrons from the surface of material, resulting in a change in the carrier concentration and leading to variations in resistance and circuit current. The sensing process can be divided into two primary steps: gas adsorption, where active sites on the material surface adsorb gas, and electron reaction, where gas interacts with electrons on the material surface. (Gong et al., 2019).

In the 2D-2D $SnSe_2/Bi_2Se_3$ heterostructure material, where the sensing material remains $SnSe_2$, the aggregation of electrons on the surface of $SnSe_2$ after heterostructure equilibrium is achieved enhances the interaction between NO_2 gas and the material. This leads to a larger change in resistance signal, thereby improving the sensitivity of the material to NO_2 gas. The synthesized $Bi_2Se_3/SnSe_2$ 2D/2D heterostructure is lamellae-stacked, which has relatively more adsorption sites and large specific surface area, which is conducive to the adsorption and desorption of NO_2. Moreover, the heterostructure exhibits significantly reduced response and recovery time duing to the enhanced electron transfer rate within the material.

4 Conclusion

In summary, $Bi_2Se_3/SnSe_2$ 2D/2D heterostructures are successfully synthesized and used for NO_2 detection. The optimized $Bi_2Se_3/SnSe_2$ heterostructure exhibited rapid response towards NO_2 gas. Compared to pure $SnSe_2$, the response time was significantly reduced from 73 to 15 s (10 ppm). The enhanced sensing performance is a direct result of the abundant n-n heterojunctions, improved interface charge transfer, and increased active sites that are inherent in the $SnSe_2/Bi_2Se_3$ heterostructure. Furthermore, the sensor displayed excellent selectivity, with a low detection limit of 10 ppb and a broad detection range from 10 ppb to 20 ppm. Furthermore, the fatigue test of the sensor after 100, 500, and 1,000 cycles bending and relaxing processes shows no significant degradation in response values. These results offer important insights for selecting materials and designing heterostructures to achieve effective room temperature gas detection in a range of applications.

Data availability statement

The original contributions presented in the study are included in the article/Supplementary Material, further inquiries can be directed to the corresponding authors.

Author contributions

SY: Conceptualization, Data curation, Investigation, Writing–original draft. CC: Data curation, Formal Analysis, Methodology, Writing–original draft. MY: Investigation, Methodology, Writing–original draft. JH: Funding acquisition, Project administration, Supervision, Writing–review and editing. YW: Funding acquisition, Resources, Supervision, Writing–review and editing.

Funding

The author(s) declare that financial support was received for the research, authorship, and/or publication of this article. This work was supported by the National Natural Science Foundation of China (Nos. 52272147 and 52072093), Heilongjiang Touyan Team (HITTY-20190034), and the Fundamental Research Funds for the Central Universities (No. 2022FRFK02015).

Conflict of interest

The authors declare that the research was conducted in the absence of any commercial or financial relationships that could be construed as a potential conflict of interest.

Publisher's note

All claims expressed in this article are solely those of the authors and do not necessarily represent those of their affiliated organizations, or those of the publisher, the editors and the reviewers. Any product that may be evaluated in this article, or claim that may be made by its manufacturer, is not guaranteed or endorsed by the publisher.

Supplementary material

The Supplementary Material for this article can be found online at: https://www.frontiersin.org/articles/10.3389/fchem.2024.1425693/full#supplementary-material

References

Ansari, H. R., Mirzaei, A., Shokrollahi, H., Kumar, R., Kim, J.-Y., Kim, H. W., et al. (2023). Flexible/wearable resistive gas sensors based on 2D materials. *J. Mater. Chem. C* 11 (20), 6528–6549. doi:10.1039/d3tc00806a

Bag, A., and Lee, N.-E. (2019). Gas sensing with heterostructures based on two-dimensional nanostructured materials: a review. *J. Mater. Chem. C* 7 (43), 13367–13383. doi:10.1039/c9tc04132j

D'Olimpio, G., Farias, D., Kuo, C.-N., Ottaviano, L., Lue, C. S., Boukhvalov, D. W., et al. (2022). Tin Diselenide ($SnSe_2$) Van der Waals Semiconductor: Surface Chemical Reactivity, Ambient Stability, Chemical and Optical Sensors. *Materials* 15 (3), 1154. doi:10.3390/ma15031154

Gong, Y., Wu, X., Zhou, X., Li, X., Han, N., and Chen, Y. (2019). High acetone sensitive and reversible P- to N-type switching NO_2 sensing properties of Pt@Ga-ZnO core-shell nanoparticles. *Sensors Actuators B-Chemical* 289, 114–123. doi:10.1016/j.snb.2019.03.085

Guo, R., Han, Y., Su, C., Chen, X., Zeng, M., Hu, N., et al. (2019). Ultrasensitive room temperature NO_2 sensors based on liquid phase exfoliated WSe_2 nanosheets. *Sensors Actuators B-Chemical* 300, 127013. doi:10.1016/j.snb.2019.127013

Han, Y., Ding, Y., Zhang, W., Zhuang, H., Wang, Z., Li, Z., et al. (2023). SnS2/Ti3C2Tx hybrids for conductometric triethylamine detection at room temperature. *Sensors Actuators B-Chemical* 381, 133360. doi:10.1016/j.snb.2023.133360

Han, Y., Huang, D., Ma, Y., He, G., Hu, J., Zhang, J., et al. (2018). Design of hetero-nanostructures on MoS_2 nanosheets to boost NO_2 room-temperature sensing. *Acs Appl. Mater. Interfaces* 10 (26), 22640–22649. doi:10.1021/acsami.8b05811

Harish, S., and Sathyakam, P. U. (2022). A review of tin selenide-based electrodes for rechargeable batteries and supercapacitors. *J. Energy Storage* 52, 104966. doi:10.1016/j.est.2022.104966

Huang, Y., Wang, K., Guo, T., Li, J., Wu, X., and Zhang, G. (2020). Construction of 2D/2D Bi_2Se_3/g-C_3N_4 nanocomposite with High interfacial charge separation and photo-heat conversion efficiency for selective photocatalytic CO_2 reduction. *Appl. Catal. B-Environmental* 277, 119232. doi:10.1016/j.apcatb.2020.119232

Joshi, N., Hayasaka, T., Liu, Y., Liu, H., Oliveira, O. N., Jr., and Lin, L. (2018). A review on chemiresistive room temperature gas sensors based on metal oxide nanostructures, graphene and 2D transition metal dichalcogenides. *Microchim. Acta* 185 (4), 213. doi:10.1007/s00604-018-2750-5

Kim, J.-H., Lee, J.-H., Mirzaei, A., Kim, H. W., and Kim, S. S. (2017). Optimization and gas sensing mechanism of n-SnO_2-p-Co_3O_4 composite nanofibers. *Sensors Actuators B-Chemical* 248, 500–511. doi:10.1016/j.snb.2017.04.029

Kim, Y., Lee, S., Song, J.-G., Ko, K. Y., Woo, W. J., Lee, S. W., et al. (2020). Highly stable contact doping in organic field effect transistors by dopant-blockade method. *Adv. Funct. Mater.* 30 (43), 2000058. doi:10.1002/adfm.202000058

Li, M., Yang, D., Jacas Biendicho, J., Han, X., Zhang, C., Liu, K., et al. (2022). Enhanced polysulfide conversion with highly conductive and electrocatalytic iodine-doped bismuth selenide nanosheets in lithium-sulfur batteries. *Adv. Funct. Mater.* 32 (26). doi:10.1002/adfm.202200529

Li, X., Jia, F., Luo, N., Cai, H., Chen, J., Ren, W., et al. (2024). Self-assembly tourmaline@BiFeO3 composites with enhanced polarization for dual-selective C3H6O and H2S detection. *Sensors Actuators B Chem.* 399, 134806. doi:10.1016/j.snb.2023.134806

Li, X., Liu, W., Huang, B., Liu, H., and Li, X. (2020). Layered $SnSe_2$ microflakes and $SnSe_2$/SnO_2 heterojunctions for low-temperature chemiresistive-type gas sensing. *J. Mater. Chem. C* 8 (44), 15804–15815. doi:10.1039/d0tc02589e

Liu, J., Hu, Z., Zhang, Y., Li, H.-Y., Gao, N., Tian, Z., et al. (2020). MoS_2 nanosheets sensitized with quantum dots for room-temperature gas sensors. *Nano-Micro Lett.* 12 (1), 59. doi:10.1007/s40820-020-0394-6

Majhi, S. M., Rai, P., and Yu, Y.-T. (2015). Facile approach to synthesize Au@ZnO core-shell nanoparticles and their application for highly sensitive and selective gas sensors. *Acs Appl. Mater. Interfaces* 7 (18), 9462–9468. doi:10.1021/acsami.5b00055

Qureshi, M. A., Shah, N. J., Hemmen, C. W., Thill, M. C., and Kruse, J. A. (2003). Exposure of intensive care unit nurses to nitric oxide and nitrogen dioxide during therapeutic use of inhaled nitric oxide in adults with acute respiratory distress syndrome. *Am. J. Crit. Care* 12 (2), 147–153. doi:10.4037/ajcc2003.12.2.147

Rathi, K., and Pal, K. (2020). Fabrication of MoSe2–graphene hybrid nanoflakes for toxic gas sensor with tunable sensitivity. *Adv. Mater. Interfaces* 7 (12). doi:10.1002/admi.202000140

Sardana, S., Singh, Z., Sharma, A. K., Kaur, N., Pati, P. K., and Mahajan, A. (2022). Self-powered biocompatible humidity sensor based on an electrospun anisotropic triboelectric nanogenerator for non-invasive diagnostic applications. *Sensors Actuators B-Chemical* 371, 132507. doi:10.1016/j.snb.2022.132507

Spirtas, R., Steinberg, M., Wands, R. C., and Weisburger, E. K. (1986). "Identification and classification of carcinogens: procedures of the chemical substances threshold limit value committee, ACGIH. American Conference of Governmental Industrial Hygienists. *ACGIH. Am. Conf. Gov. Industrial Hygienists." Am. J. public health* 76 (10), 1232–1235. doi:10.2105/ajph.76.10.1232

Wang, H., Xu, M., Ji, H., He, T., Li, W., Zheng, L., et al. (2023). Laser-assisted synthesis of two-dimensional transition metal dichalcogenides: a mini review. *Front. Chem.* 11, 1195640. doi:10.3389/fchem.2023.1195640

Wang, L., Jackman, J. A., Ng, W. B., and Cho, N.-J. (2016). Flexible, graphene-biocomposite for highly sensitive, real-time molecular detection. *Adv. Funct. Mater.* 26 (47), 8623–8630. doi:10.1002/adfm.201603550

Wang, L., Jackman, J. A., Park, J. H., Tan, E.-L., and Cho, N.-J. (2017). A flexible, ultra-sensitive chemical sensor with 3D biomimetic templating for diabetes-related acetone detection. *J. Mater. Chem. B* 5 (22), 4019–4024. doi:10.1039/c7tb00787f

Xu, T., Han, Y., Lin, L., Xu, J., Fu, Q., He, H., et al. (2019). Self-power position-sensitive detector with fast optical relaxation time and large position sensitivity basing on the lateral photovoltaic effect in tin diselenide films. *J. Alloys Compd.* 790, 941–946. doi:10.1016/j.jallcom.2019.03.293

Yang, S., Yin, H., Wang, Z., Lei, G., Xu, H., Lan, Z., et al. (2023). Gas sensing performance of In_2O_3 nanostructures: a mini review. *Front. Chem.* 11, 1174207. doi:10.3389/fchem.2023.1174207

Yang, Y., Zhu, M., Zhang, H., Wang, B., Chen, C., Li, J., et al. (2024). Room temperature gas sensor based on rGO/Bi_2S_3 heterostructures for ultrasensitive and rapid NO_2 detection. *J. Chem. Eng.* 490. doi:10.1016/j.cej.2024.151872

Yang, Z., Lv, S., Zhang, Y., Wang, J., Jiang, L., Jia, X., et al. (2022). Self-Assembly 3D porous crumpled MXene spheres as efficient gas and pressure sensing material for transient all-MXene sensors. *Nano-Micro Lett.* 14 (1), 56. doi:10.1007/s40820-022-00796-7

Zappa, D., Galstyan, V., Kaur, N., Arachchige, H. M. M. M., Sisman, O., and Comini, E. (2018). Metal oxide -based heterostructures for gas sensors" - a review. *Anal. Chim. Acta* 1039, 1–23. doi:10.1016/j.aca.2018.09.020

Zhang, J., Liu, X., Neri, G., and Pinna, N. (2016). Nanostructured materials for room-temperature gas sensors. *Adv. Mater.* 28 (5), 795–831. doi:10.1002/adma.201503825

Zheng, Y., Zhou, T., Zhang, C., Mao, J., Liu, H., and Guo, Z. (2016). Boosted charge transfer in SnS/SnO_2 heterostructures: toward high rate capability for sodium-ion batteries. *Angew. Chemie-International Ed.* 55 (10), 3408–3413. doi:10.1002/anie.201510978